Proceedings of 2009 ASME Pressure Vessels and Piping Division Conference
PVP2009
July 26-30, 2009, Prague, Czech Republic

PVP2009-77821

PLASTIC DEFORMATION AND VIBRATION IN A FLUID-FILLED TUBE SUBJECT TO AXIAL IMPACT

Kazuaki Inaba and Joseph E. Shepherd*
Graduate Aeronautical Laboratories
California Institute of Technology
Pasadena, California, 91125
Email: joseph.e.shepherd@caltech.edu

ABSTRACT

The goal of the present study is to examine the coupling of large-amplitude (including plastic deformation) flexural waves and precursor waves in water-filled, thin-wall (1.6 mm) steel tubes. To do this, we have compared the coupling created by exciting the stress waves in water versus in the tube wall. To examine the case of coupling from water to the tube, we used projectile impact on the water surface to create pressure waves in the water propagating along the tube axis. We have tested mild steel tubes using a steel impactor accelerated to speeds of up to 80 m/s using an air cannon to strike a polycarbonate buffer placed on top of the water surface within the tube. Strain gages measure hoop and longitudinal stresses at selected locations and a pressure gage measures the reflected pressure at the bottom of the tube. To examine the coupling from the stress waves in the tube to pressure waves in the water, we excited stress waves by axial impact on the tube along using a Hopkinson bar coupled to the tube without making contact with the water. For direct impact on the water surface, propagating plastic deformation flexural waves with more than 2% hoop strain were obtained at an impact speed of 80 m/s. The maximum hoop strain was observed just below the bottom surface of the buffer as a bulge with 16% hoop strain. Hoop and longitudinal strains indicate a steep elastic front followed by a gradual plastic deformation. Initially, the plastic deformation is dominant but the peak amplitude decays as the wave propagates. Since the plastic deformation wave travels much slower than the elastic waves, the initial flexural wave fronts propagate at 1350 m/s and are close to the wave speed of the Korteweg's elastic theory of water hammer. Stress waves propagated at 5400 m/s in the tube wall and caused a 1-2 MPa pressure fluctuation in the water. Comparing strain histories to those of tubes without water, we observe that the coupling to the water damps high frequency vibrations and reduced peak amplitudes while maintaining the ratio of hoop and longitudinal strains.

NOMENCLATURE

a Radius of pipe
c Velocity of sound in water
c_0 Velocity of sound in tube wall
c_1, c_2 Skalak's phase velocities
c_K Korteweg's phase velocity
E Young's modulus of tube material
h Thickness of tube wall
K Bulk modulus of fluid
m Mass of tube per unit surface area
P_D Driver (reservoir) pressure

*Address all correspondence to this author.

Copyright © 2009 by ASME

V_B Buffer velocity immediately after impact
V_P Projectile impact velocity
ρ Density of steel
ρ_0 Density of water
ν Poisson's ratio

INTRODUCTION

The present study is motivated by problem of marine structure response and survivability under shock loading. An underwater detonation produces a shock wave followed by a bubble pulse related to the expansion of the products of detonation. The shock loading and subsequent response of a structure is a type of fluid-structure interaction (FSI) that has been extensively studied for the normal impact of an explosively generated shock wave on a plate. Other aspects of fluid-solid coupling relevant to marine structural response to explosive loading are the coupling of flexural waves in plates and shells with the stress waves in the wave propagating perpendicular to the solid surface. This type of coupling is also widely encountered in the industrial problem of water hammer [1–3]. To investigate FSI experimentally, we are using projectile impact and water-filled tubes as shown in Fig. 1. This configuration has been used by many other researchers to examine diverse issues such as cavitation [4], metal forming [5], and underwater shock wave simulations [6, 7].

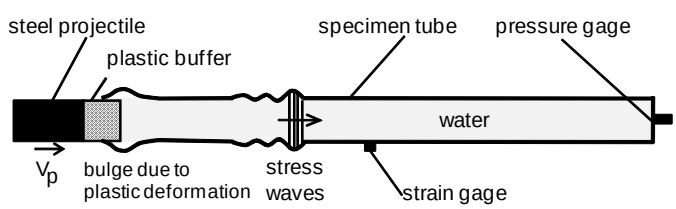

Figure 1. Schematic diagram of axi-symmetric water-in-tube configuration for generation of shell flexural waves coupled with stress waves propagating in water.

As discussed by Inaba and Shepherd [8], the extent of fluid-solid coupling in this geometry is determined by the parameter $Ka/(Eh)$, where K is bulk modulus of fluid, a is radius of a tube, E is Young's modulus of the tube, and h is the wall-thickness of the tube. Unlike the case of normal impact of a shock wave, the coupling depends only on material properties and is independent of flow behind the shock. The linear elastic theory of water hammer by Skalak [9] reveals that the impact transient will generate two waves. A primary or slow wave, which contains the main disturbance in fluid pressure and tube strain, moves at the Korteweg speed of classical water hammer. The precursor or fast wave is a much smaller amplitude (200 times smaller in hoop and 10 times smaller in longitudinal strain) disturbance than the primary wave that travels with the thin-plate wave speed of the tube wall. If the primary wave has positive pressure and hoop strain, then the precursor will be a longitudinal strain tension wave.

One of the predictions in the Skalak's theory is that the coupled (elastic) stress waves produced by FSI travel with velocities that are independent of the projectile speed. However, the peak amplitude of the stress waves is predicted to be a linear function of the projectile velocity. We have examined these predictions by carrying out experiments over a range of projectile speeds for various materials (metal and composites) and both thin and thick-wall tubes [8, 10]. In our previous experiments, the projectile velocities were just barely high enough to exceed the elastic-plastic-proportional limit and plasticity did not play a major role. In the present paper, we report experiments with much faster impact speeds to create significant plastic deformation and examine the evolution of the resulting stress waves with time. In order to do these experiments, we had to create a new facility for launching high speed projectiles and use very ductile specimens so that we could have large deformations without rupturing the tubes.

EXPERIMENTAL APPARATUS AND TEST PROCEDURE

Gas Gun

We designed and built an air cannon (Fig. 2) that is capable of projectile exit velocities more than 200 m/s and a barrel diameter of 50 mm. The air cannon is mounted vertically above a specimen tube filled with water. The 1.5 kg steel projectile is accelerated by compressed air using driver (reservoir) pressures, P_D, up to 16 MPa. Referring to Fig. 3, the launching procedure for the projectile is as follows:

1. The projectile with gland seals is loaded into the barrel and the space between the top of the piston and the gun barrel is evacuated to hold the projectile at the top end of the barrel.
2. The air reservoir is filled to the desired pressure. The gun barrel has four ports to the reservoir space and the gland seals of the projectile initially prevent air from entering through these ports.
3. The vacuum line is closed and a remotely-operated valve connects the air reservoir to the evacuated region above the projectile.

Copyright © 2009 by ASME

4. Once compressed air introduced at the top of the barrel pushes the projectile sufficiently downward to uncover the ports, the compressed air in the reservoir rushes in and rapidly accelerates the projectile downward.

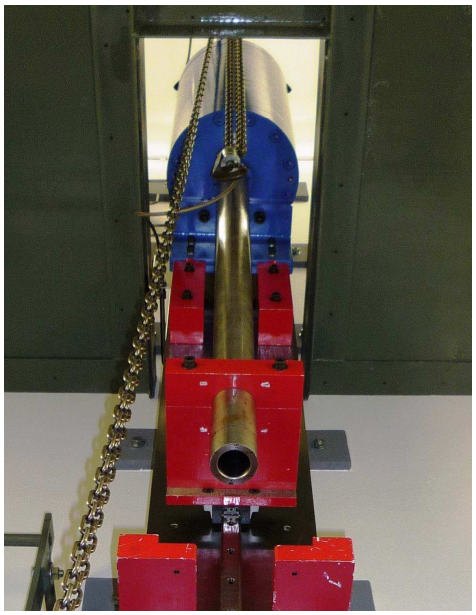

Figure 2. GALCIT 2-in gas gun mounted vertically in Explosion Dynamics Laboratory.

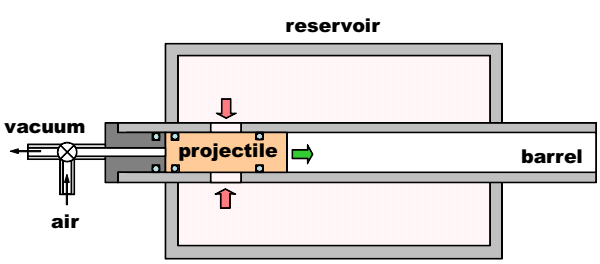

Figure 3. Schematic diagram of the projectile launching mechanism.

The projectile is not completely ejected from the barrel when it impacts a polycarbonate buffer placed on the water surface which is just below the top of the specimen tube (as shown in Fig. 4). A gland seal is used to prevent water moving through the clearance space between the buffer and tube. In this fashion, the stress waves due to the impact of the projectile are transmitted directly to the water surface inside the specimen tube. This prevents the projectile from impacting the specimen tube directly and enables us to measure the wave velocities without interference from axial waves created by the projectile impact on the tube itself.

Table 1. Test Matrix.

Shot	Tube	Length [m]	P_D [MPa]	V_B [m/s]
048	#9	1.715	0.50	36.4
050	#10	1.715	0.95	46.3
052	#11	1.715	1.75	62.7
073, 074	#8	0.902	Free fall	8.0*
101	#12	0.902	1.75	62.5
103	#13	0.902	2.50	71.4

*calculated from Hopkinson bar data

The impact generated stress waves in the water cause the tube to deform and the resulting coupled fluid-solid motion propagates down the tube. The deformation of the tube is measured by strain gages oriented in the hoop and longitudinal directions and the pressure in the water is measured by a piezoelectric transducer (Fig. 4) mounted in an aluminum fitting sealed to the bottom of the tube. The bottom of the tube is fastened to an aluminum bar mounted in a lathe chuck that is placed directly on the floor. The top and bottom of the tube were reinforced with a circumferential clamp (visible at the top of the tube in Fig. 14) to prevent radial expansion and fluid leakage.

By impacting the tube rather than the water, we have studied the generation of fluid motions due to structural vibration in the specimen tube. Figure 5 shows a schematic of the test setup for these structure-fluid interaction tests. A Hopkinson bar replaces the polycarbonate rod as a buffer and the bar is attached directly to the specimen top. The water top surface is 25.4 mm below the Hopkinson bar bottom, and therefore axial impact does not transmit from the bar directly to the water.

Test Conditions and Specimens

The two tube lengths are tested: one long, 1.715 m; and one short, 0.902 m. All specimen tubes are cold-rolled electrically-welded mild-steel (C1005-1006) and have a wall thickness of

Copyright © 2009 by ASME

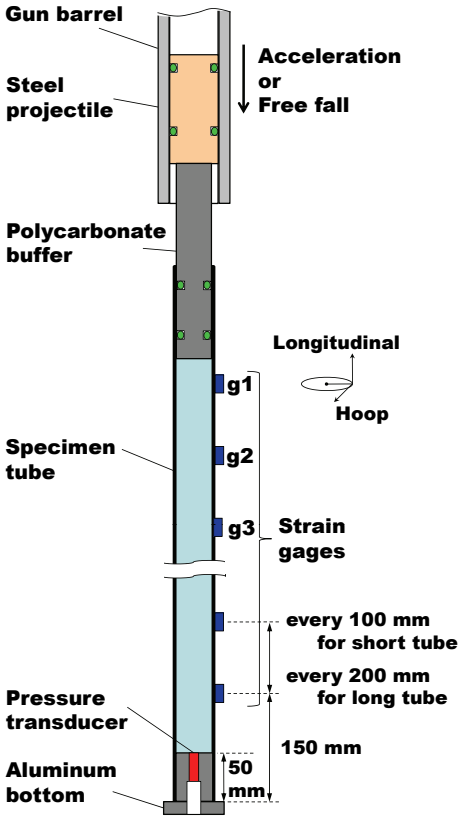

Figure 4. Test specimen tube with projectile, buffer, pressure transducer, and strain gages.

1.59 mm and inner diameter 38.0 mm. Each test specimen is instrumented with strain gauges at 200 mm increments for long tubes and 100 mm increments for short tubes. A high-speed video camera (Vision Research Phantom v7.3) is used to observe the buffer motion due to the projectile impact and determine the buffer speeds and the surface position of buffer during experiments.

The projectile speed at the exit of the barrel and initial buffer speed were varied by using different pressures in the gas reservoir. Initial driver gas conditions and measured buffer projectile speeds are given in Table 1. Buffer speeds are determined from video images over 10 mm of motion. In preliminary experiments, we determined the correlation of projectile speed with reservoir pressure. We also found experimentally that the initial buffer speed is 10-30% lower than the projectile speed, depending on the reservoir pressure with higher differences at higher

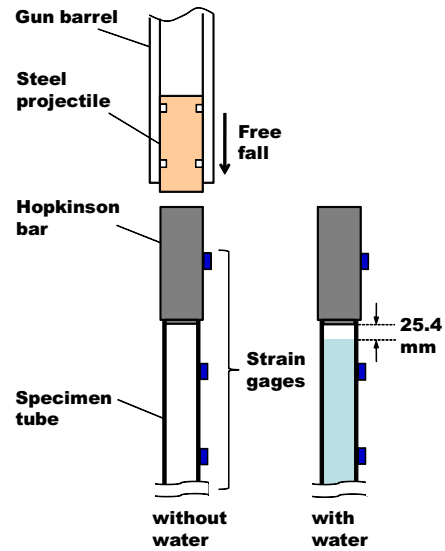

Figure 5. Schematic diagram of test setup for structure-induced fluid motion.

pressures.

An elastic strain wave is excited in the tube wall when the impact speed (buffer speed) is sufficiently low. The test setup is usually checked first in this regime by simply dropping a lubricated projectile (without gland seals) onto the buffer. Once the instrumentation is checked in the elastic regime, the projectile is launched using compressed air. By using sufficiently high launch speeds, we are able to transition from the elastic to the plastic regime and the peak amplitude of the initial hoop strain wave readily exceeds the nominal elastic proportional limit of 2 *m*strain [8].

RESULTS AND DISCUSSION

Plastic deformation Waves

Hoop strain and pressure histories are shown in Fig. 6 for a 62.7 m/s impact measured at locations g1 (bottom trace) to g7. The location g1 is closest to the buffer bottom surface and the top of a series of strain gages. The bottom gauge is mounted 150 mm from the end of the specimen; the other gages are spaced at 200 mm increments. The top trace is the pressure history and since this is obtained in the solid end wall, the pressure values are enhanced due to the substantial effects of reflection at the aluminum-water interface. In Fig. 6, the signal baselines are offset proportional to the distance between the gages so that we can

Copyright © 2009 by ASME

also interpret the trajectories of signal features by considering the ordinate as space location as well as signal amplitude. For example, the lines labeled 5219 m/s and 1356 m/s indicate the leading edge of the precursor and the primary (main) stress wave front that is initiated by the impact. The positions of the leading edge are detected by signal processing using a MATLAB program to determine when the strain magnitude becomes larger than an arbitrary threshold (0.2-0.5 *m*strain for the primary wave and 0.02-0.05 *m*strain for the precursor wave). A MATLAB program is also used to obtain the slope of the linear function using the method of least squares. Despite the very large (up to 16%) permanent deformations that occur in this test, the observed speeds of the precursor and main wave front are in reasonable agreement with the model predictions [9] of 5226 m/s and 1337 m/s . This good agreement is apparently a consequence of the limited deformation that takes place in the precursor and initial primary waves, making the elastic assumption of the Skalak model a reasonable approximation.

As shown in Fig. 6, the pressure wave is clearly connected to the primary wave, and decays very slowly after the arrival of the primary wave. The disturbances after the arrival of the precursor wave are much smaller in magnitude than the primary wave. Longitudinal strain histories are measured at the same locations g1-g6 and are shown in Fig. 7. By comparison with the hoop histories, the precursor wave is more distinct while the primary wave front is less so in the longitudinal histories.

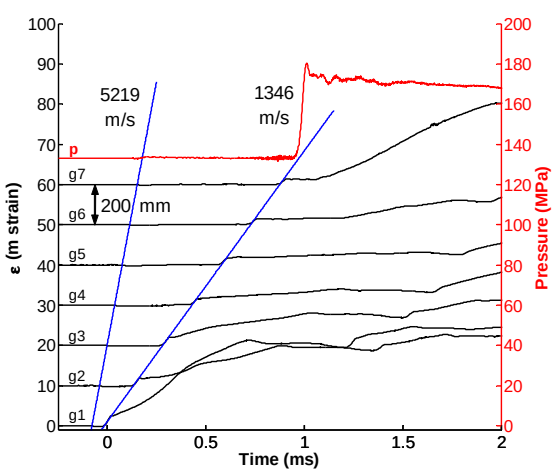

Figure 6. Hoop strain and pressure histories for shot 052, long tube, $V_B = 62.7$ m/s.

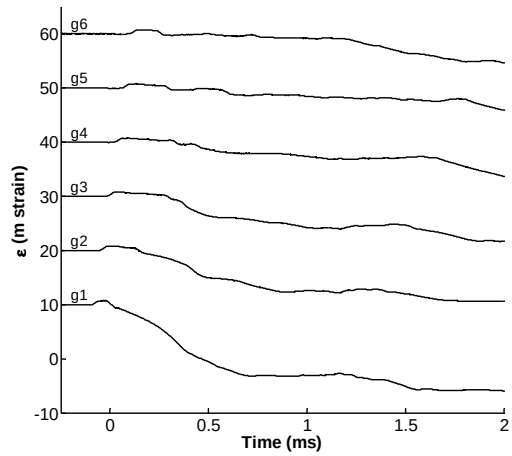

Figure 7. Longitudinal strain histories for shot 052, long tube, $V_B = 62.7$ m/s.

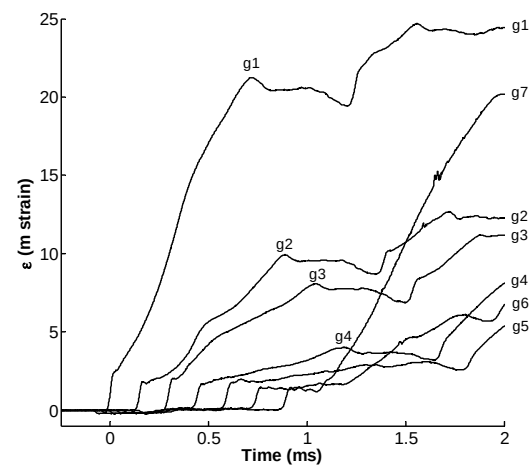

Figure 8. Evolution of plastic wave hoop strain histories for shot 052, long tube, $V_B = 62.7$ m/s.

Hoop strain histories are shown without displacement of the baselines (Fig. 8) in order to directly compare the evolution of the wave amplitude with time. The main stress wave propagates with limited amplitude at high speed and is followed by a much slower

Copyright © 2009 by ASME

plastic deformation wave with changing amplitude. A relatively long time is required to reach the ultimate plastic deformation as compared to the initial elastic deformation waves. The situation appears to be very similar to that of uniaxial stress waves in shock compression [11]: An elastic precursor wave with an amplitude given by the proportional limit travels at the elastic longitudinal wave speed in front of a lower speed plastic wave with a continuous increase in strain (stress) up to the final level of permanent deformation. In the present case, significant attenuation of the plastic wave is observed with increasing distance from the impact point. This occurs in uniaxial shock compression testing due the attenuation of a following expansion wave.

In the case of FSI plastic waves, we speculate that there are multiple factors for the attenuation of the plastic wave amplitude including not only the expansion wave but also the radial motion of the tube wall and the energy absorption due to plastic work. Figures 9 and 10 show the strain histories for shots 050 and 048, with two lower buffer speeds. In all three cases, peaks of the elastic front gradually decay from 2.0 *m*strain to 1.5 *m*strain. The time of peak plastic deformation increases with increasing buffer speed. One explanation for the evolution of the peak deformation time is that this occurs when pressure inside the tube becomes smaller than the pressure needed to exceed the yield stress of the tube wall. The sudden increase of the hoop strain after the first peak is caused by the rebound and second impact of the projectile on the buffer.

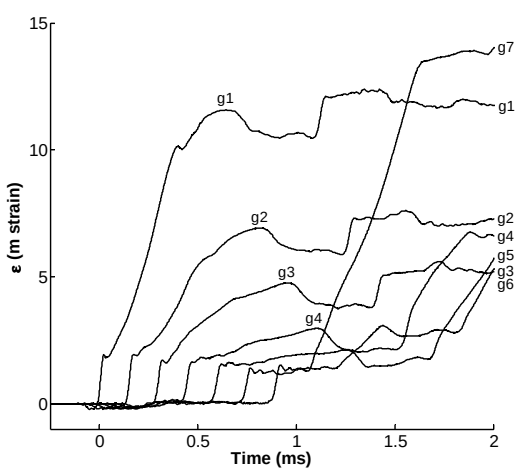

Figure 9. Evolution of plastic wave hoop strain histories for shot 050, long tube, $V_B = 46.3$ m/s.

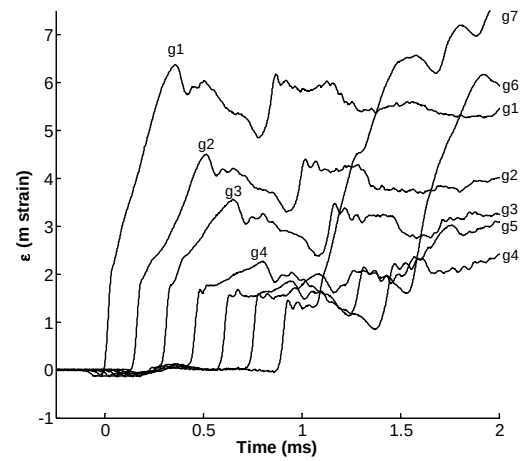

Figure 10. Evolution of plastic wave hoop strain histories for shot 048, long tube, $V_B = 36.4$ m/s.

With increasing projectile exit velocity, the buffer is displaced further into the tube and the projectile may be ejected from the barrel exit. For safety, we performed the faster impact tests with shorter tubes that were enclosed by plywood panels and bullet-resistant polycarbonate plate. Figure 11 shows hoop strain and pressure histories for shot 103, a shorter tube prepared in the same manner as the one used in Fig. 6 with strain gages installed at 100 mm increments. The primary wave speed is close to the Korteweg speed while the precursor wave speed is slightly slower than the Skalak's prediction. Strain histories are initially the same as those in Fig. 6 but the signals abruptly terminate when the gages and/or connections are destroyed by the large amplitude deformations. This effect is more pronounced in the shorter tubes than the longer ones because gages mounted on shorter tubes are located at a closer distance to the buffer than for the longer tubes.

Figures 12 and 13 show the evolution of the hoop strain histories with the characteristic sharp elastic front followed by a smooth plastic deformation. The strain histories are terminated after the time that the gages are destroyed. An additional strain gage is added in shot 103 so that the history g1 in Fig. 12 corresponds to location of history g2 in Fig. 13. The results are qualitatively similar for shots 101 and 103 and the additional gage shows clearly that the highest strains are produced just below the bottom of the buffer. The maximum residual strain is 254.2 *m*strain (25.4%) in shot103 and 167.4 *m*strain (16.7%) in

Copyright © 2009 by ASME

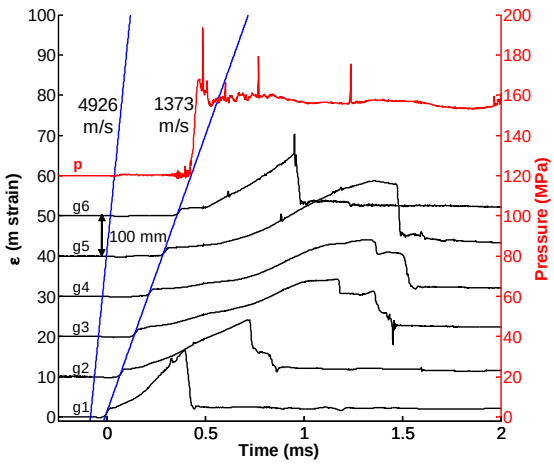

Figure 11. Hoop strain and pressure histories for shot 103, short tube, $V_B = 71.4$ m/s.

shot101.

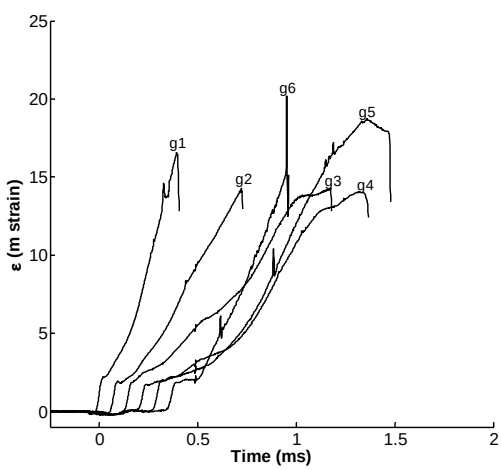

Figure 12. Evolution of plastic wave hoop strain histories for shot 103, short tube, $V_B = 71.4$ m/s.

After the shot, the tubes have two prominent bulges due to plastic deformation near the buffer bottom, Fig. 14a, and the tube bottom (due to stress wave reflection from the closed end)

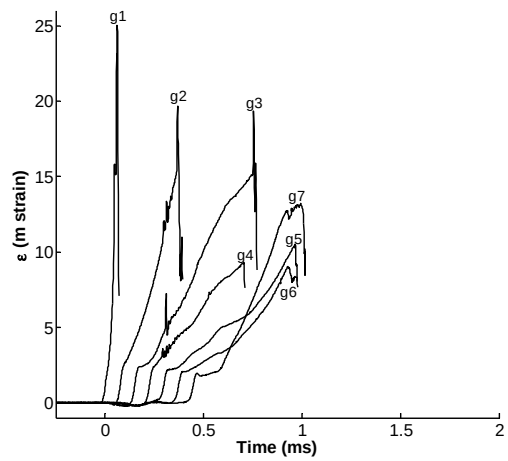

Figure 13. Evolution of plastic wave hoop strain histories for shot 101, short tube, $V_B = 62.5$ m/s.

Fig. 14b. Photographic observations during the test were made with the high-speed video camera and selected frames as shown in Fig. 15. The first 3-4 frames correspond to time period during which we can obtain strain gage histories. The bulge shown in Fig. 14a starts to develop just after the impact and keeps growing until the buffer reverses the initial downward direction. The last frame is taken at approximately the time of the start of buffer ascent.

The relationships between the primary and precursor wave speeds and the buffer speeds are summarized in Fig. 16. Both wave speeds appear to be essentially independent of the buffer speed with a possible small decrease in precursor speed with increasing buffer speed. As the buffer speed is increased, the amplitude of the precursor wave becomes larger while the initial hoop strain is fixed by the proportional limit of the tube. The precursor wave places the tube into tension longitudinally and into compression in the hoop direction, compressing the fluid and inducing pressure waves in the fluid. We refer to this as structure-fluid interaction (SFI) and have carried out a separate study of this effect that is described in the subsequent section.

Using the measured initial buffer speeds, we can estimate using standard shock wave interaction methods [11] the peak pressure in the water due to the buffer impact, and the reflected pressure off the aluminum bottom end. The graphical interpretation of these interactions is shown in the pressure-particle (P-u) diagram drawn for shot 103 in Fig. 17. Neglecting the FSI, a shock pressure of 92.5 MPa is created by the impact, the ac-

Copyright © 2009 by ASME

Figure 14. Post-test photographs of specimen bulges for shot 103, short tube, $V_B = 71.4$ m/s: (a) near the buffer bottom; (b) near the specimen bottom end.

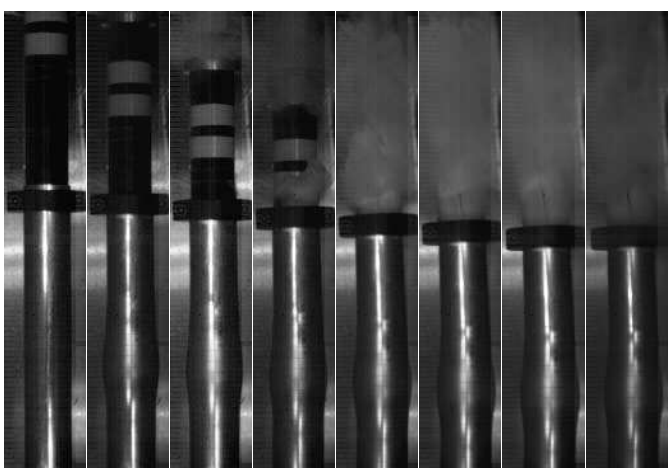

Figure 15. Series of frames from high-speed video showing the development of the bulge of the specimen tube near the buffer bottom surface after the projectile impact in shot 103. The interval between images is 735 μs.

tual value will be smaller to the interaction with the tube wall expansion. The reflected pressure measured at the bottom end is estimated to be about 1.75-times larger (162 MPa) than the actual post-shock pressure in the fluid. We can estimate the post-shock pressure from this relationship and the values are listed in Table 2. The hoop stress shown in the table is estimated by neglecting inertia and bending stresses $\sigma_{hoop} \approx P_{estimated} a/h$, which is the approximation used in the simplest theory of water hammer. Since the reflected pressure is almost the same in all cases, the estimated hoop stress is also the same. This hoop stress is consistent with the yield stress (300-400 MPa) of the mild steel at the observed strain rates of 10^1 to 10^2 s^{-1}. Therefore, we conclude that after the wave has reached the bottom of the tube, the stress wave amplitude is determined by the magnitude of the yield stress of the tube wall.

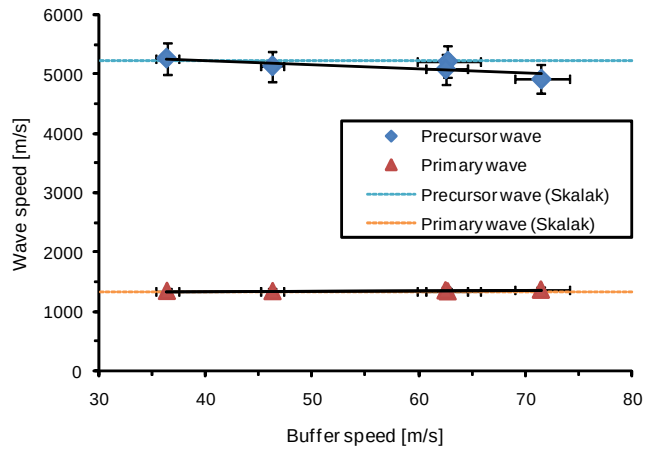

Figure 16. Primary and precursor wave speeds vs. buffer speed (impact speed).

Table 2. Summary of experimental results.

Shot	Strain rate [1/s]	$P_{reflected}$ [MPa]	$P_{estimated}$ [MPa]	σ_{hoop} [MPa]
048	38.7	46.5	26.6	333
050	54.2	47.0	26.9	337
052	50.0	47.3	27.0	339
101	75.6	49.3	28.2	353
103	67.9	48.1	27.5	345

Tube Vibration and Structure-Fluid Interaction

In the previous section, we observed that the longitudinal precursor wave is coupled to the fluid motion, which we termed

Copyright © 2009 by ASME

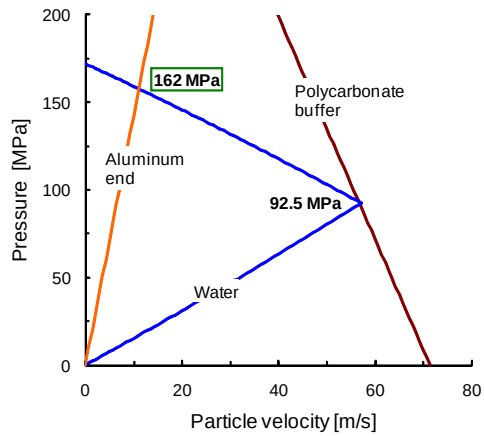

Figure 17. P-u diagram of shock interactions at water-polycarbonate buffer interface, and water-aluminum bottom interface for shot 103. The intersection points give the ideal states neglecting the FSI.

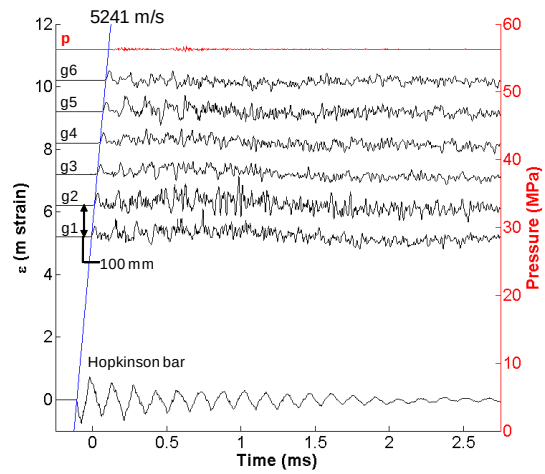

Figure 18. Hoop strain and pressure histories shown together with Hopkinson bar data (longitudinal strain) for shot 073, no water case, short tube, free fall, $V_B = 8.01$ m/s.

structure-fluid interaction since the longitudinal structure motion is the limiting case of a purely structural mode. To examine the SFI effect, we performed experiments with and without water in the specimen tube, comparing strain histories and oscillation frequencies.

Figure 18 shows the hoop strain and pressure histories together with the longitudinal strain history on the Hopkinson bar for shot 073, w/o water and using a freely-falling projectile for the impact event. The effective buffer speed, 8.0 m/s, is calculated from the measured longitudinal strain pulse in the Hopkinson bar (4340 alloy steel) and is slightly faster than our previous free fall tests. The high-frequency oscillations are dominant in the hoop histories and the hoop motion appears less correlated to the Hopkinson bar forcing than the longitudinal motion. The wave front speed is 5241 m/s and fairly close to the sound speed of the bar mode in the tube wall. Longitudinal strain histories are given in Fig. 19. Since the Hopkinson bar directly impacts the specimen tube, the longitudinal strain is larger than the hoop strain and without water in the tube, the hoop strain is generated only through the Poisson effect and coupling due to end effects. The longitudinal oscillations initially follow the excitation of the Hopkinson bar data and after a number of reverberations, lower-amplitude high-frequency oscillations become dominant after 1.0 ms. A long period oscillation of about 500 Hz can be observed in the longitudinal strain. We speculate that this is associated with the beam bending motions of the tube due to slightly off-axis excitation of the Hopkinson bar.

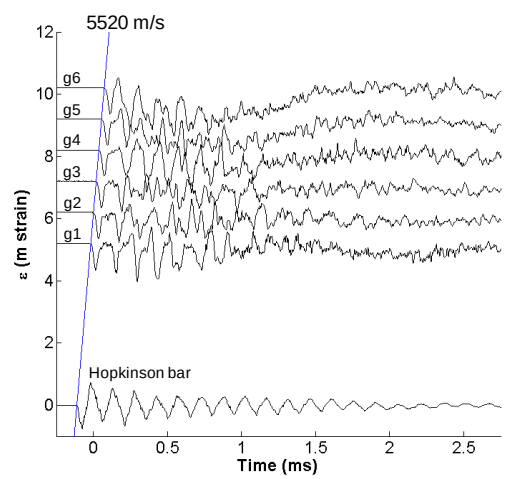

Figure 19. Longitudinal strain histories shown together with Hopkinson bar data (longitudinal strain) for shot 073, no water case, short tube, free fall, $V_B = 8.01$ m/s.

The spectrograms of the hoop and longitudinal strain histories are calculated using fast Fourier transform (FFT) methods and are presented in Figs. 20 and 21. The spectrograms enable us to visualize how the power spectrum evolves with time and

Copyright © 2009 by ASME

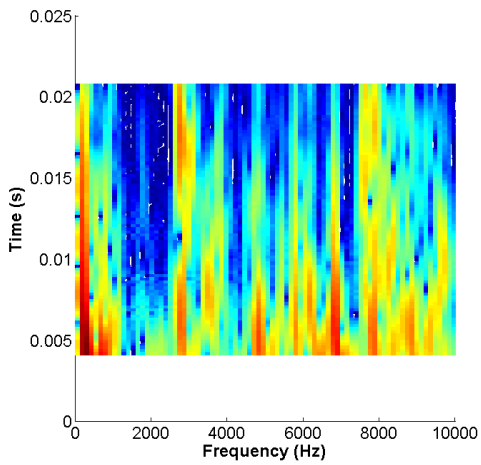

Figure 20. Spectrogram of hoop strain history at g5 for shot 073.

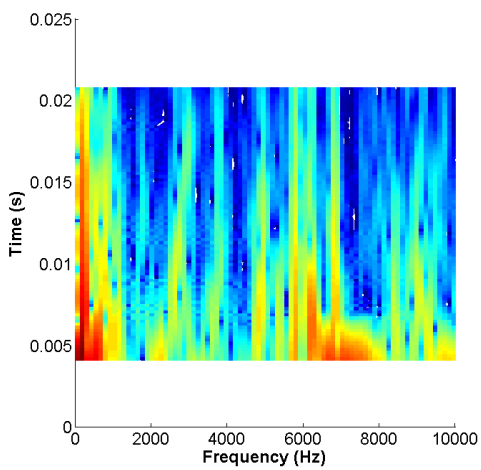

Figure 21. Spectrogram of longitudinal strain history at g5 for shot 073.

we can observe the transition from the initial forcing input to the natural oscillations. The forcing input from the Hopkinson bar has a characteristic frequency of about 7000-8000 Hz. This signal is apparent in the longitudinal spectrogram before 0.7 ms. Natural frequencies of the specimen tube, assuming purely bar mode longitudinal oscillations, are estimated [12] to be

$$f = \frac{n}{2l}\sqrt{\frac{E}{\rho}} \quad (n = 1, 2, 3, \ldots) \tag{1}$$

where l is the specimen length. For example: n =1, f = 2858 Hz; n =2, f = 5715 Hz; n =3, f = 8753 Hz. Considering the free vibrations of a shell structure [12], there are a very large number of modes and examining the spectrograms, it is clear that many modes other than the longitudinal oscillation are excited by the projectile impact. In general, wave propagation in a shell structure is dispersive [13] and the longitudinal impact on a cylindrical shell (see Section 4.3 of Graff [13]) will create not just a simple strain pulse predicted by the one-dimensional theory but just as in the case of bar impact, there will be a substantial oscillatory component.

When the specimen tube is filled with water, the effects of structure-fluid interaction can observed in the strain histories and frequency spectra. Figures 22 and 23 show the hoop and longitudinal strain histories for shot 074 with a water-filled tube. Compression (extension) of the tube in the longitudinal direction causes expansion (compression) of the tube in the radial direction due to the Poisson effect. These radial oscillations of the tube excite pressure oscillations in the fluid inside the tube. The peak amplitude of these oscillations is 2-3 MPa, much smaller than the values obtained with direct impact on the water surface. Energy transfer to the water and the damping effects of viscosity result in smoother signals and smaller oscillation amplitudes in the water-filled cases as compared to the empty tubes. However, there is little effect on the speed of the strain front due to the weak excitation of the coupled modes in the SFI case. The measured wave speeds for hoop and longitudinal strains are 5275 m/s and 5433 m/s, essentially the same as observed in the case without water.

The effect of adding water can be most prominently observed in the spectrograms of hoop and longitudinal strains, shown for shot 074 in Figs. 24 and 25. Following the decay of the initial input from the Hopkinson bar, only a few modes remain excited after 0.7 ms. The main frequencies appear to be associated with the first (2858 Hz) and second (5715 Hz) mode of the longitudinal bar oscillation and the low frequency bending mode at about 500 Hz. Theoretical analysis of fluid-filled shells predict four axisymmetric branches with an infinite number of possible frequencies for small-amplitude vibration [14–16]. An analysis of the initial value problem and consideration of dissipation will be needed to determine which modes would be expected

Copyright © 2009 by ASME

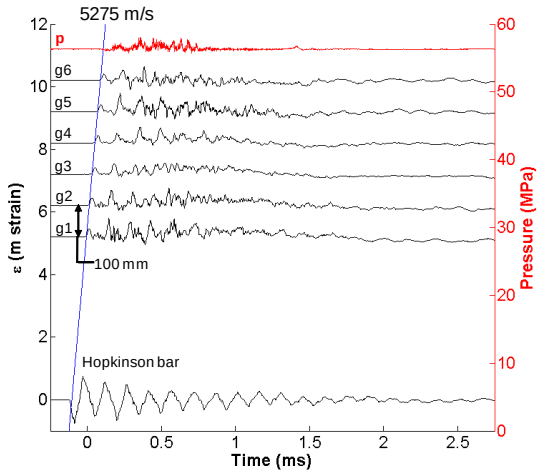

Figure 22. Hoop strain and pressure histories shown together with Hopkinson bar data (longitudinal strain) for shot 074 with water case, short tube, free fall, $V_B = 8.01$ m/s.

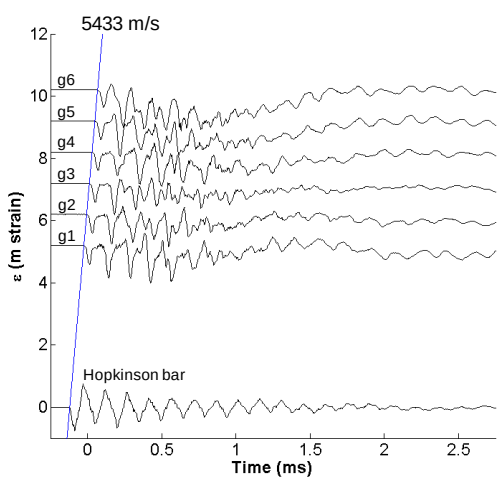

Figure 23. Longitudinal strain histories shown together with Hopkinson bar data (longitudinal strain) for shot 074 with water case, short tube, free fall, $V_B = 8.01$ m/s.

to dominate in the present situation. We have not considered this yet in our studies.

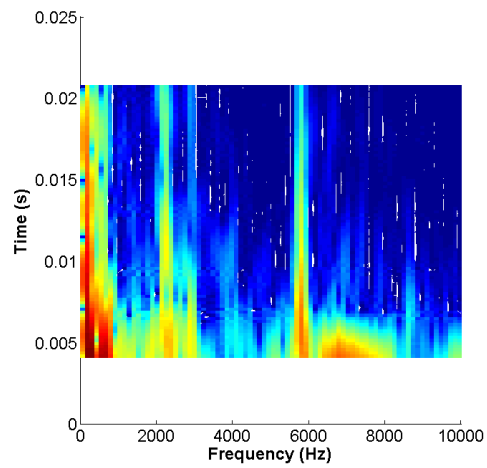

Figure 24. Spectrogram of hoop strain history at g5 for shot 074.

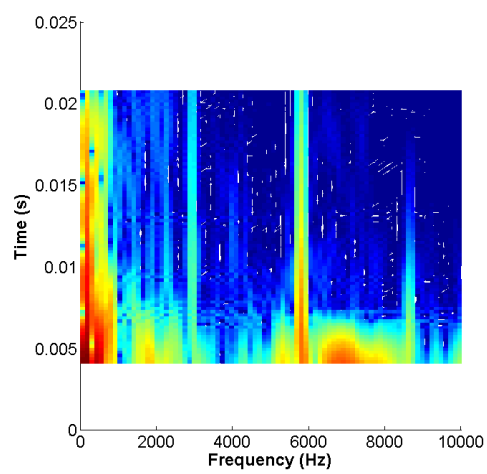

Figure 25. Spectrogram of longitudinal strain history at g5 for shot 074.

CONCLUSION

We have demonstrated that axial projectile impact on the fluid can be used to create propagating plastic deformation waves in ductile, thin-wall, fluid-filled tubes. The plastic deformation waves we observe are superficially analogous to the waves observed in projectile impact on homogeneous samples. Our observations of hoop strain reveal that the plastic waves consist of a sharp hoop strain front traveling at close to the classical Ko-

Copyright © 2009 by ASME

rteweg speed followed by a slower plastic deformation wave. The initial strain front is limited in amplitude by the yield stress of the tube metal but the subsequent plastic deformations were as high as 25% immediately downstream of the impact point. Attenuation of the plastic deformation wave occurred relatively rapidly so that under the conditions of the present tests, the large-amplitude deformation was confined to locations near impact or wave reflection. Although the speed of the deformation wave front was determined by the FSI, the extent of plastic deformation was controlled by the impact velocity. This indicates that our technique is capable of generating sufficiently large amplitude stresses to make this useful for testing marine structure response to impulse loading. In companion studies, we have used this method to examine the response of tubes fabricated from composite materials.

Impact on the tube structure alone demonstrates that the coupling from the structure into the fluid is much weaker and very low amplitude pressure waves in the fluid are created due to the Poisson coupling effect. As expected, the fluid is effective at damping the shell vibrations and the longitudinal strain waves are the most persistent features following the decay of the initial impact-generated waves. Direct impact on the fluid rather than the tube is clearly the method of choice for creating large-amplitude hoop strains and fluid pressures.

ACKNOWLEDGMENT

This research was sponsored by the Office of Naval Research, DOD MURI on Mechanics and Mechanisms of Impulse Loading, Damage and Failure of Marine Structures and Materials (ONR Grant No. N00014-06-1-0730), program manager Dr. Y. D. S. Rajapakse. We thank Tomohiro Nishiyama for his help in conducting experiments. Mike Kaneshige of Sandia National Laboratories provided substantial assistance with the gun design.

REFERENCES

[1] Watters, G. Z., 1984. *Analysis and Control of Unsteady Flow in Pipelines*. Butterworth Publishers, MA.

[2] Wylie, E. B., and Streeter, V. L., 1993. *Fluid Transients in Systems*. Prentice-Hall, Inc., NJ.

[3] Wiggert, D. C., and Tijsseling, A. S., 2001. "Fluid transients and fluid-structure interaction in flexible liquid-filled piping". *Applied Mechanics Reviews,* **54**(5), pp. 455–481.

[4] Trevena, D., 1987. *Cavitation and Tension in Liquids*. Adam Hilger.

[5] Skews, B., Kosing, E., and Hattingh, R., 2004. "Use of a liquid shock tube as a device for the study of material deformation under impulsive loading conditions". *Proc. Instn. Mech. Engrs. J. Mechanical Engineering Science,* **218**, pp. 39–51.

[6] Espinosa, H., Lee, S., and Moldovan, N., 2006. "A novel fluid structure interaction experiment to investigate deformation of structural elements subjected to impulsive loading". *Experimental Mechanics,* **46**, p. 805824.

[7] Deshpande, V. S., Heaver, A., and Fleck, N. A., 2006. "An underwater shock simulator". *Proc. R. Soc. A,* **462**, pp. 1021–1041.

[8] Inaba, K., and Shepherd, J. E., 2008. "Flexural waves in fluid-filled tubes subject to axial impact". In Proceedings of the ASME Pressure Vessels and Piping Conference. July 27-31, Chicago, IL USA. PVP2008-61672.

[9] Skalak, R., 1956. "An extension to the theory of water hammer". *Transactions of the ASME,* **78**, January, pp. 105–116.

[10] Inaba, K., and Shepherd, J. E., 2008. "Impact generated stress waves and coupled fluid-structure responses". In Proceedings of the SEM XI International Congress & Exposition on Experimental and Applied Mechanics. June 2-5, Orlando, FL USA. Paper 136.

[11] Meyers, M. A., 1994. *Dynamic behavior of materials*. John Wiley & Sons.

[12] Blevins, R. D., 2001. *Formulas for natural frequency and mode shape*. Krieger.

[13] Graff, K. F., 1975. *Wave motion in elastic solids*. Dover.

[14] Fuller, C. R., and Fahy, F. J., 1982. "Characteristics of wave propagation and energy distributions in cylindrical elastic shells filled with fluid". *J. Sound Vibration*, pp. 501–518.

[15] Sinha, B. K., Plona, T. J., Kostek, S., and Chang, S.-K., 1992. "Axisymmetric wave propagation in fluid-loaded cylindrical shells". *J. Acoust. Soc. Am.,* **92**, August.

[16] Pinnington, R. J., 1997. "The axisymmetric wave transmission properties of pressurized flexible tubes". *Journal of Sound and Vibration,* **204**, pp. 271–289.

Copyright © 2009 by ASME